Nuclear Cardiology, Part IV: Viability

Liesbet Mesotten, Alex Maes, Anne-Sophie Hambye, Hendrik Everaert, Vera Van den Maegdenbergh, Philippe Franken and Luc Mortelmans

Nuclear Medicine, Catholic University of Leuven, Leuven; Nuclear Medicine, Middelheim Hospital, Antwerp; and Nuclear Medicine, Free University of Brussels, Brussels, Belgium

Objective: After reading Part IV of this series of nuclear cardiology articles, the reader should be able to describe: (a) the differences between SPECT and PET techniques; (b) the various radiopharmaceuticals and imaging protocols used for detecting viability with SPECT; (c) the different radiopharmaceuticals and imaging protocols used for detecting viability with PET; and (d) the imaging patterns observed after reconstructing myocardial images.

Key Words: myocardial viability; SPECT; PET; imaging protocols; thallium-201; technetium-99m-sestamibi; iodine-123-IPPA; iodine-123-BMIPP; nitrogen-13-ammonia; fluorine-18-FDG; carbon-11-acetate

J Nucl Med Technol 1999; 27:93–102

The differentiation of viable from nonviable myocardium in patients with chronic coronary artery disease (CAD) and left ventricular (LV) dysfunction is clinically important (*1*). It is generally accepted that impaired LV function is not necessarily an irreversible process. Regional myocardial contractile dysfunction at rest has been observed to improve after restoration of adequate blood flow. The ventricular function can significantly improve even in patients who have had markedly reduced LV ejection fraction before intervention.

Abnormalities of ventricular function may be due to persistently depressed blood flow, prolonged myocardial cellular dysfunction after transient ischemia, or myocardial infarction. This article reviews the role of nuclear medicine in monitoring myocardial viability.

Myocardial stunning is a condition of prolonged but reversible dysfunction after a period of acute ischemia followed by reperfusion (*2–5*). Acute coronary occlusion followed by thrombolysis (*6*), a period of unstable angina (*7,8*) or exercise-induced ischemia (*9*) can cause this situation. In all these situations the acute reduction of perfusion results in an acute reduction in contraction that may persist for days to weeks after restoration of blood flow (*10*).

Hibernation describes a situation of chronically reduced myocardial perfusion at rest associated with an impairment in contractile function, which can be reversed after revascularization (*11,12*). The reduction of contractile function may be a protective response of the myocardium to meet the reduced supply of oxygen and substrates, leading to a new situation of perfusion-contraction matching, to prevent cell death (*13,14*). Vanoverschelde et al. (*15*) have postulated that the majority of myocardial regions of patients with chronic myocardial dysfunction have subnormal to normal perfusion. It is possible that repeated episodes of ischemia can induce a chronic reduction in contractility (*16,17*). This phenomenon is referred to as repetitive stunning (*15*).

Cardiac imaging techniques that evaluate myocardial viability on the basis of myocardial perfusion, cell membrane integrity, metabolic activity and residual coronary reserve have been developed with clinical success. These methods provide great precision in assessing viable myocardium. The clinical purpose is to predict which myocardial regions are viable and will improve systolic function after revascularization.

Echocardiography with low-dose dobutamine infusion to increase systolic contraction in dyssynergic regions is an alternative method for assessing myocardial viability (*18*). Nuclear medicine imaging uses two techniques: SPECT and PET.

SPECT TECHNIQUES

Thallium-201

The myocardial cell wall is a semipermeable membrane that selectively allows some substances to pass into and out of the cell. This membrane has a sodium-potassium pump mechanism that actively transports Na^+ to the outside and K^+ to the inside. The energy for this process is provided by the breakdown of adenosine triphosphate (ATP). ATP is an important intracellular compound whose breakdown yields energy.

Conventional SPECT using ^{201}T1 as a perfusion tracer can be used to predict myocardial viability (*19*). The mechanism of ^{201}Tl uptake in perfused myocardial cells is parallel to the mechanism of K^+ uptake (*20*). Myocardial uptake of ^{201}Tl is most dependent on the functioning of the sodium-potassium pump. After the uptake phase, there is a continuous washout of

For correspondence or reprints contact: Alex Maes, MD, PhD, Dept. of Nuclear Medicine, UZ Gasthuisberg, Herestraat 49, 3000 Leuven, Belgium.

the tracer from the myocardium. Thallium-201 is continually clearing from normally perfused myocardium and recirculating in the vascular compartment. This process of continuous exchange forms the basis of ^{201}Tl redistribution.

Redistribution of ^{201}Tl is seen if serial imaging is performed after an early stress injection. Fill-in of an ischemic defect is due to more rapid washout from normal segments and slower washout from ischemic segments. In addition, reuptake of ^{201}Tl into low-flow myocardium from persistent blood levels also occurs (*21*). Myocardial necrosis shows an initial defect after ^{201}Tl injection and no delayed ^{201}Tl redistribution. Different ^{201}Tl protocols have been described for detecting myocardial viability.

Thallium-201 has a long physical half-life of 73 h. It produces low-energy photons, which are below the optimal range for gamma camera imaging. The emitted x-rays (69–80 keV, 98%) are used for detection, not the gamma rays (135–167 keV, 2–8%). These x-ray photons are easily attenuated by body tissues, often resulting in apparent perfusion defects, which are due to breast, chest wall or diaphragmatic attenuation (*22*).

Possible Protocols for Thallium-201 Viability Imaging: Stress Protocols. In our department imaging is performed with a tomographic triple-head gamma camera, equipped with low-energy high-resolution (LEHR) collimators. Each detector rotates over a 120° orbit acquiring 24 projections per head, 30 s per projection in a 64 × 32 matrix and a zoom of 1.2 resulting in a pixel size of 5.93 mm. The raw data of only 180° (RAO → LAO) are reconstructed by filtered backprojection using a Hanning filter (0.6 cycles/cm) into transaxial slices, long-axis and short-axis slices. The posterior projections of LAO → RAO cannot be used because of the attenuation.

Myocardial ^{201}Tl scintigraphy is most often performed in conjunction with exercise stress (bicycle, treadmill or pharmacological). This test permits the detection of stress-induced ischemia and simultaneous assessment of regional myocardial viability.

The traditional ^{201}Tl imaging protocol involves injecting 90–130 MBq ^{201}Tl at peak exercise on a treadmill or bicycle. The long half-life of ^{201}Tl limits the dose that can be injected. A fasting state is recommended for the stress test. The washout of the tracer makes the starting time of the acquisition after stress critical. The acquisition should not be started earlier than 10 min postinjection to reduce the frequency of the upward creep artifact.

The uptake of ^{201}Tl in the heart reaches a maximum 5 min postexercise. Perfusion defects observed on the ^{201}Tl images obtained after exercise indicate transient ischemia or scar, or a combination of both. Delayed images obtained after 3–4 h make it possible to differentiate viable from nonviable myocardium. If redistribution occurs, the myocardium is viable. In addition, irreversible defects on stress-redistribution ^{201}Tl scintigraphy do not always represent scarred myocardium. Persistent defects with not more than 25–50% reduction in ^{201}Tl counts, compared with normal counts on poststress and delayed images, also are indicative of viability (*23*).

The serum tracer concentration influences the ^{201}Tl redistribution. The delayed uptake is mainly due to continued exposure of the myocardial cell membrane to the tracer levels recirculating into the blood from other organs. Late redistribution imaging at 24 h can demonstrate redistribution not clearly seen on 4-h redistribution images. A limitation of 24-h delayed imaging is the suboptimal count statistics that increase noise in images. At least a 50% longer imaging time should be used to enhance counting statistics.

There are 3 different reinjection technique protocols. All 3 protocols start with a stress test. In the first protocol a reinjection of ^{201}Tl is performed immediately after the stress test if an area of uptake of less than 50% is seen. The redistribution images are performed after 4 h. In the second protocol reinjection also is performed immediately after obtaining the stress images and followed by imaging 1 h after reinjection. This procedure may eliminate the need for additional 3–4-h redistribution imaging and offers reduced imaging time and may increase patient throughput (*23*).

In the third protocol the redistribution images are taken 4 h after stress imaging and a reinjection of ^{201}Tl is performed, if there is an area of decreased uptake of less than 50% on the redistribution images. The reinjection images are taken after 24 h.

The detection of viability by ^{201}Tl reinjection may be explained by the hypothesis that a sufficient concentration of ^{201}Tl in the blood is necessary to allow the visualization of the redistribution of ^{201}Tl in severe perfusion defects. Redistribution in a ^{201}Tl perfusion defect will never occur if ^{201}Tl blood levels are too low (*24*).

Possible Protocols for Thallium-201 Viability Imaging: Rest Protocols. For rest ^{201}Tl scintigraphy, imaging is performed 15 min after injection of the tracer. Overnight fasting for this protocol is not necessary. With this protocol, 2 SPECT studies are acquired: a resting SPECT at 15 min postinjection and a 4-h redistribution SPECT (*23*). There is substantially slower washout of ^{201}Tl over time from chronically underperfused regions, as compared with more rapid ^{201}Tl washout from nonischemic regions. An initial perfusion defect at rest that shows subsequent redistribution is indicative for viability.

Technetium-99m-Labeled Agents

Technetium-99m-labeled perfusion agents can be used to detect myocardial ischemia and distinguish viable from irreversibly damaged myocardium. The ^{99m}Tc isonitriles and ^{99m}Tc-tetrofosmin seem to be the most promising of this group of agents for determining myocardial viability.

Myocardial uptake of ^{99m}Tc-sestamibi is proportional to the regional blood flow. In the cell ^{99m}Tc-sestamibi is concentrated in the mitochondria. Technetium-99m-sestamibi uptake appears to be dependent on cell membrane integrity and mitochondrial respiration (*25*). Despite the differences in kinetics between ^{99m}Tc-sestamibi and ^{201}Tl, the regional myocardial uptake of the two tracers is similar. Minimal redistribution of ^{99m}Tc-sestamibi allows an uncoupling of time of injection from the time of imaging.

Initial studies claim that resting ^{99m}Tc-sestamibi SPECT studies can be used to obtain information on myocardial viability. It is stated that quantified ^{99m}Tc-sestamibi activity 1 h after rest injection is similar to redistribution ^{201}Tl activity. This

suggests that ^{99m}Tc-sestamibi is more than a pure flow tracer (*26*,*27*).

Imaging Protocol for Technetium-99m-Sestamibi SPECT. Sixty minutes before the start of the acquisition, 555 MBq ^{99m}Tc-sestamibi are injected at rest and flushed with 10 mL saline. Approximately 30 min after injection, patients drink 2 glasses of whole milk to enhance hepatic clearance of the isotope. In our department cardiac imaging is performed on a triple-head system. Images are acquired with a low-energy high-resolution collimator. Each detector rotates over a 360° orbit acquiring a total of 72 projections, 15 s per projection in a 64 × 32 matrix and a zoom of 1.2, resulting in a pixel size of 5.93 mm. A 20% window centered on the 140-keV photopeak is used. The projections are processed with a Butterworth filter with a cutoff of 0.52 cycles/cm and an order of 5 and are reconstructed with a ramp filter into transaxial slices, long-axis and short-axis slices.

Gated SPECT Imaging. Gated SPECT imaging evaluates ventricular function at rest during a myocardial perfusion study. It gives an appreciation of wall thickening, wall motion and left ventricular volumes. The higher count statistics and better imaging characteristics of ^{99m}Tc make it the most preferred radiopharmaceutical for gated studies.

The differentiation between viable and nonviable myocardium is possible with this technique. In patients with perfusion defects, gated SPECT imaging is helpful in detecting myocardial viability and differentiating with attenuation artifacts. A perfusion defect still showing wall thickening and/or motion can be identified as a viable region. Wall motion and photon activity are the basis for viability (*28–30*).

Imaging Protocol for Technetium-99m-Sestamibi Gated SPECT. In our department imaging is performed with a rotating triple-head gamma camera, equipped with a high-resolution parallel-hole collimator. The patient is injected with 740 MBq ^{99m}Tc-sestamibi in the fasting state at rest. Thirty minutes postinjection 2 glasses of milk are given to decrease gallbladder activity. Sixty minutes postinjection the patient is positioned comfortably on the scan table and 3 electrodes are placed on the left arm, right arm and right leg to obtain a clear R-R wave signal. Special care must be taken to establish a stable ECG for each patient. Once a stable ECG pattern is obtained, the gate interval is calculated. Each detector rotates over a 360° orbit acquiring a total of 72 projections in step-and-shoot mode in a 64 × 32 matrix and a zoom of 1.2, resulting in a pixel size of 5.93 mm. Each cardiac cycle is divided into 8 frames. Acquisition time per projection is determined by the individual heart rate and results in an effective acquisition time of about 1 min for each projection (the 3 heads summed). Beats within 10% of the mean length are accepted. The raw sestamibi projections are processed with a two-dimensional Butterworth filter with a cutoff of 0.4 cycle/cm and an order of 10, and are reconstructed with a ramp filter into transaxial slices, long-axis and short-axis slices.

Physical Limitations. Attenuation is a major problem in interpreting cardiac SPECT images. Attenuation means that photons interact with electrons of the surrounding tissue, lose some energy and change their direction. These photons will not be detected by the system. The heart is surrounded by tissues of different densities (breast, lung, liver) causing nonuniform attenuation of the photons.

No global solution is available, however, an individual correction for each patient is needed. A transmission scan of the thorax is acquired and an individual attenuation map is calculated. The emission images are corrected with this map (*31*,*32*). Attenuation correction offers some benefits, but there are also some limitations.

Artifacts can be caused by misalignment between the emission and the transmission scans when they are acquired consecutively. A shift between transmission and emission results in nonhomogeneous activity distribution (*33–36*). Another source of artifacts is the truncation of the patient during transmission. This occurs when the patient's body is too large and falls out of the field of view between transmission source and fanbeam collimator (*34–36*).

Photons emitted by the radiopharmaceutical interact with the electrons of the surrounding tissue and lose some energy. These scattered photons are detected at a lower energy, as compared to the original energy, and are detected at the place of interaction. An important portion of scattered photons is detected by the window around the photopeak.

One of the scatter correction methods is the triple-energy window method. This method uses a window above and below the usual one. The measured photopeak can be split up into a primary photopeak, or the unscattered peak, and a scatter peak (*34*,*37*).

Free Fatty Acid Analogs

Cardiac work is highly energy consuming. In normal, nonischemic conditions with a good oxygen supply, oxidation of circulating long-chain fatty acids is the major source of cardiac energy, at least in the fasting state. This process is oxygen-consuming and very sensitive to the regional blood oxygen content. Decreased oxygen supply (hypoxia) as encountered in myocardial regions perfused by narrowed vessels, will result in a dramatic reduction of β-oxidation, replaced by catabolism of glucose (glycolysis) to produce the necessary energy. This feature constitutes the basis of the scintigraphic methods for viability assessment with radiolabeled metabolic tracers, relying mostly on a comparison between a flow tracer and either fatty acid or glucose analogs. In an attempt to image oxidative metabolism, ^{123}I-labeled fatty acids have been developed, of which the 2 most frequently used are the iodophenyl pentadecanoic acid (IPPA) and the 3-methyl iodophenyl pentadecanoic acid (BMIPP).

With IPPA, a straight-chain free fatty acid, β-oxidation occurs as for native free fatty acids and image quality is not stable over the course of time. To overcome this problem, the structure of the fatty acids has been modified by adding a ''branch'' to the straight chain, thereby precluding complete β-oxidation, significantly prolonging the cardiac retention time and thus allowing stable high-quality SPECT imaging. BMIPP is currently the most widely used of these branched free fatty acid analogs in clinical practice.

BMIPP Kinetics. BMIPP behaves primarily as a flow tracer, and its initial uptake depends on regional blood flow. After

injection, the ^{123}I-BMIPP is rapidly extracted by the myocardium and is actively transported into the cells where it undergoes the initial steps of β-oxidation. In animal studies it has been demonstrated that the uptake of BMIPP is closely related to the intracellular concentration of the adenosine triphosphate required to initiate fatty acid oxidative catabolism (*38*). Afterwards, because of the presence of its branched group, further catabolism is avoided almost completely and the partially metabolized BMIPP is incorporated into the intracellular lipid storage pool (*39*). Only a limited proportion is oxidized and is probably responsible for the limited washout observed in clinical studies (about 5.6–13.0% between 20 min and 3 hr postinjection at rest (*40*), while backdiffusion of nonmetabolized BMIPP is very limited (±2.1% in dogs). Although it does not follow the complete catabolic pathways of native free fatty acids, BMIPP can be used to image their metabolism.

In pathological conditions of decreased oxygen supply, the amount of backdiffused, nonmetabolized BMIPP increases significantly, resulting in a decreased uptake in the ischemic area compared to the normal regions. The severity of this defect is related significantly to the severity of coronary stenoses or to regional wall motion abnormalities (*41*).

Clinical Applications for Viability. BMIPP can be used to assess flow and metabolism consecutively with a single injection when early (dynamic) imaging is followed by a delayed acquisition because its uptake is primarily dependent on regional blood flow (*42*). In the setting of myocardial viability studies, however, most published data rely on the comparison between BMIPP and a perfusion tracer.

In acute myocardial infarctions, a strong association has been reported between a ''negative'' mismatch (BMIPP less than perfusion) and jeopardized but viable myocardium and between a matched decreased uptake of both tracers and nonviable tissue. Compared to dobutamine stress echocardiography, the combined use of BMIPP and ^{99m}Tc-sestamibi has demonstrated a similar accuracy to predict functional recovery after acute myocardial infarction (*43*).

In chronic infarctions, the number of segments with less BMIPP than perfusion has been shown to be the strongest predictor of adverse cardiac events at follow-up (*44*), while the presence of a negative mismatch has the same significance regarding residual contractile reserve during dobutamine stress echocardiography (*45*) or functional recovery after revascularization than in the acute phase. A ''positive'' mismatch with more BMIPP than perfusion, altough rarely encountered, also has been described by some authors and seems associated with unstable conditions or severe wall motion abnormalities (*46*).

PET currently is the gold standard for viability studies. BMIPP results have been validated against this technique. Compared to ^{11}C-palmitate, which demonstrates fatty acid metabolism, or to ^{18}F-fluorodeoxyglucose, concordant findings were noted in 81% and 82%, respectively (*47*).

From an analysis of the literature, it can be concluded that the combined evaluation of BMIPP and perfusion reliably differentiates between viable and nonviable myocardial tissue in both acute and chronic phases of ischemic heart disease. It is also a useful tool for viability assessment with SPECT. A negative mismatch with less BMIPP than perfusion identifies viable tissue, whereas a matched decreased uptake of both tracers corresponds to myocardial scar.

Acquisition Parameters. For the perfusion study, either ^{201}Tl or a ^{99m}Tc-labeled compound can be injected at rest, using a standard acquisition protocol. However, because of the similar physical characteristics of ^{123}I and ^{99m}Tc, the use of ^{99m}Tc-labeled perfusion tracers should be recommended whenever possible.

For the BMIPP study, a dose of 111–148 MBq ^{123}I-BMIPP is injected at rest after administration of 400–600 mg potassium perchlorate to block thyroidal uptake of free iodine. Until now at least 6 h fasting before tracer administration was recommended, although it has been suggested recently that image quality is at least as good in nonfasting patients.

Unless dynamic acquisition is performed, the patient is allowed to eat during the 20–30-min waiting time. The acquisition is performed using a 360° orbit, noncircular body contoured and step-and-shoot protocol. Ideally, the camera should be equipped with medium-energy collimators (*48*). Otherwise, low-energy, all-purpose collimators are preferred to high-resolution because of a better signal-to-noise ratio. Using a triple-head gamma camera, 90 projections (30/head) of 60 s duration are acquired using a 128 × 128, 128 × 64 or 64 × 64 matrix. Because of a significantly high scatter level in the BMIPP images, scatter correction should be applied if possible (*49*). If desired, a second (delayed) acquisition can be performed between 1 and 3 h after the first using the same parameters, to calculate washout rates. Reconstruction is performed with appropriate filtered backprojection in a 64 × 64 matrix using the 360° data.

PET TECHNIQUES

PET is known to accurately identify viable tissue myocardium in patients with impaired left ventricular function. PET is a technique that enables the measurement of small amounts of radiopharmaceuticals labeled with positron-emitting radioisotopes. To produce these positron-emitting radionuclides, a nuclear particle accelerator (cyclotron) is used. The cyclotron-produced positron-emitting radionuclides ^{15}O, ^{13}N, ^{11}C and ^{18}F are very useful for incorporation into compounds of physiologic interest. A positron emitted from a nucleus will annihilate with an electron and produce simultaneously two 511-keV gamma rays traveling in opposite directions which can be detected by PET. The superiority of PET over other nuclear imaging techniques is based on its high sensitivity, high spatial resolution, the availability of attenuation correction and absolute quantification of tracer uptake (*50*).

Viability of the myocardium in patients with CAD can be evaluated by the combined measurement of regional myocardial perfusion and metabolism. In this context, viable myocardium refers to areas of dysfunctional myocardium recovering after revascularization. To differentiate dyssynergic but viable myocardium from necrotic tissue, it is necessary to integrate information on myocardial perfusion and glucose uptake. Myocardial blood flow is often studied using radioactive-

labeled ammonia ($^{13}NH_3$) while myocardial metabolism can be investigated using ^{18}F-fluorodeoxyglucose (FDG).

Nitrogen-13-Ammonia

Nitrogen-13-ammonia is one of the most frequently used PET tracers to quantify myocardial blood flow. Nitrogen-13-ammonia has a 10-min physical half-life and high tissue retention fractions (*51*).

Imaging Protocol for Nitrogen-13-Ammonia. A 2-min rectilinear scan for positioning the heart within the field of view and a 15-min transaxial transmission scan using a ^{68}Ge ring for photon attenuation correction is performed before each study. In our department the dose of $^{13}NH_3$ to be injected is calculated by dividing the patient's weight by 4 up to a maximum amount of 20 mCi (370 MBq). The $^{13}NH_3$ in 5 mL saline followed by a 20-mL flush of saline is infused slowly with a pump at a constant rate of 10 mL/min. The acquisition is started simultaneously with the injection of $^{13}NH_3$. In each patient 21 dynamic frames are recorded (12×10 s, 4×30 s, 3×2 min, 1×3 min, 1×7 min). The total acquisition time is 20 min.

The first frames of the perfusion studies are reconstructed using a Hanning filter with a cutoff frequency of 0.3. A summed frame is constructed using frames 18–21. The long axis of the left ventricle is indicated manually on the summed frame. The myocardial image is resampled into 16 radial slices. The radial slices are delineated using an algorithm developed in our department, resulting in an endocardial and an epicardial contour and a basal plane. From the radial slices, a corresponding set of short-axis slices is constructed (*52*,*53*). The delineation is used to construct a polar map. For every pixel of the polar map, the corresponding position in the left ventricular wall is known (Fig. 1). A three-compartment model is used to calculate absolute flow values (*54*,*55*).

Fluorine-18-Fluorodeoxyglucose

In the fasting state, free fatty acid (FFA) levels are high, whereas glucose and insulin levels are low. After eating, the glucose and insulin levels rise. The increase in insulin levels induces an enhanced myocardial glucose uptake and inhibits the oxidation of FFA. In the postprandial state, glucose becomes the preferred substrate for cardiac energy production (*56*). Under ischemic conditions with decreased oxygen delivery, oxidative metabolism of FFAs is decreased and exogenous glucose becomes the preferred substrate for the myocardium (*57*). Increased glucose utilization relative to blood flow is one of the metabolic hallmarks of myocardial ischemia.

The initial uptake of FDG is related closely with glucose uptake. The clinical applicability of FDG is based on the effective intracellular trapping after phosphorylation to FDG-6-phosphate. In contrast to glucose-6-phosphate, FDG-6-phosphate is not a substrate for further metabolism.

Imaging with ^{18}F-FDG is widely accepted as a metabolic marker of viable myocardium. Although adequate myocardial perfusion is a key factor for tissue viability, measurement of flow values alone does not permit categorizing myocardial segments as being viable or nonviable. Hypoperfused but viable

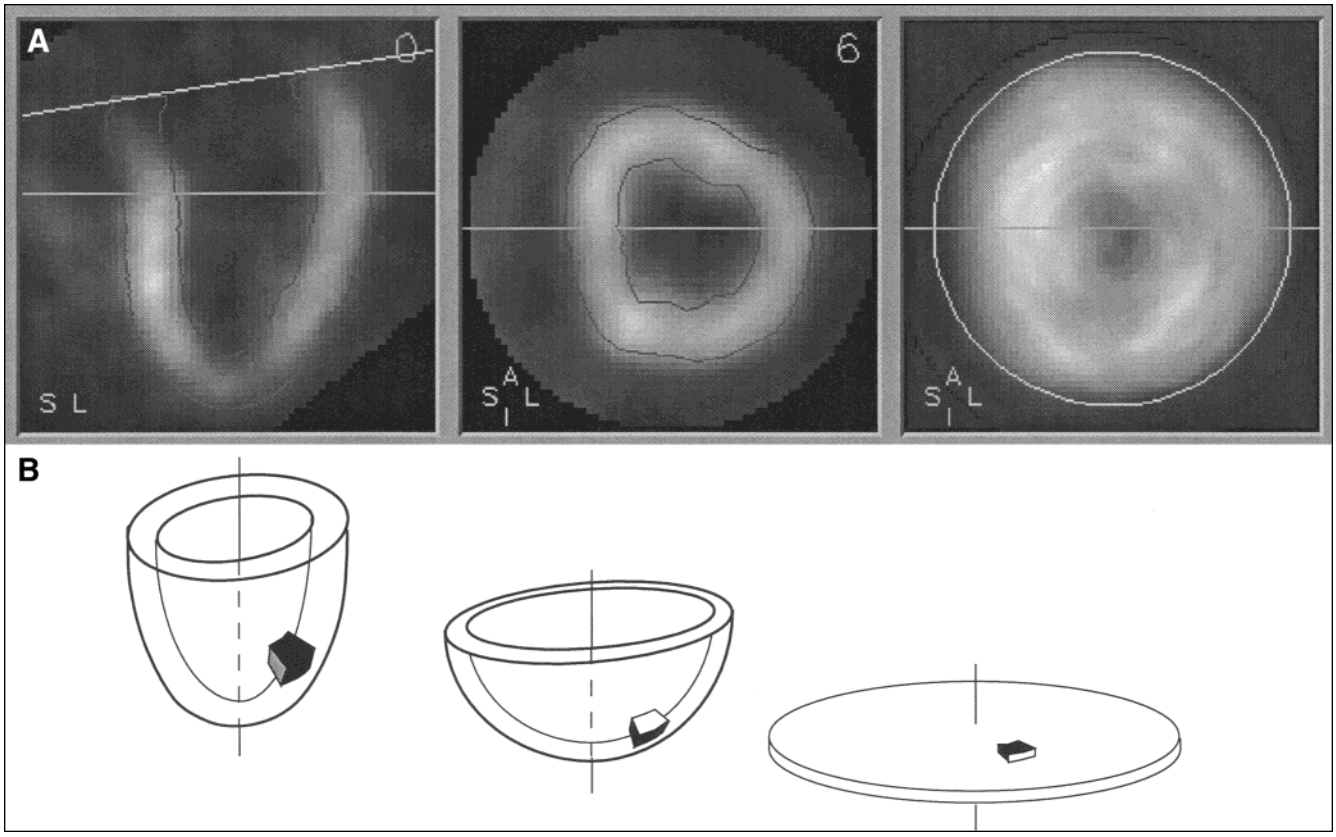

FIGURE 1. (A) An example of radial and short-axis slices with the corresponding polar map. (B) A three-dimensional delineation of the left ventricular wall to construct a polar map.

segments of the myocardium can be identified from necrosis using PET. A PET viable pattern consisting of hypoperfusion with relatively preserved FDG uptake (PET mismatch) or normal flow and metabolism is an indicator of viability, whereas a combined reduction of both parameters (PET match) suggests necrosis (transmural or nontransmural). Patients with CAD and a PET viable pattern are known to improve function after revascularization, while a necrosis PET pattern (concordant decrease of flow and FDG uptake) predicts the absence of contractile recovery after bypass surgery (*19*,*58*) (Fig. 2). The identification of viable, reversibly dysfunctional myocardial segments with PET has important clinical implications.

Imaging Protocol for Fluorine-18-FDG. The amount of FDG to be injected is calculated by dividing the patient's weight by 8 with a maximum of 10 mCi (370 MBq) ^{18}F administered. Two different types of acquisition are possible: a static acquisition and a dynamic acquisition. A dynamic acquisition is performed if quantification of the data is necessary. This quantification provides valuable information about the regional glucose utilization in the myocardium.

Since glucose uptake varies considerably under fasting and postprandial conditions, much attention has been paid to the optimal conditions during which FDG imaging should be performed. There are 3 possibilities to optimize the glucose

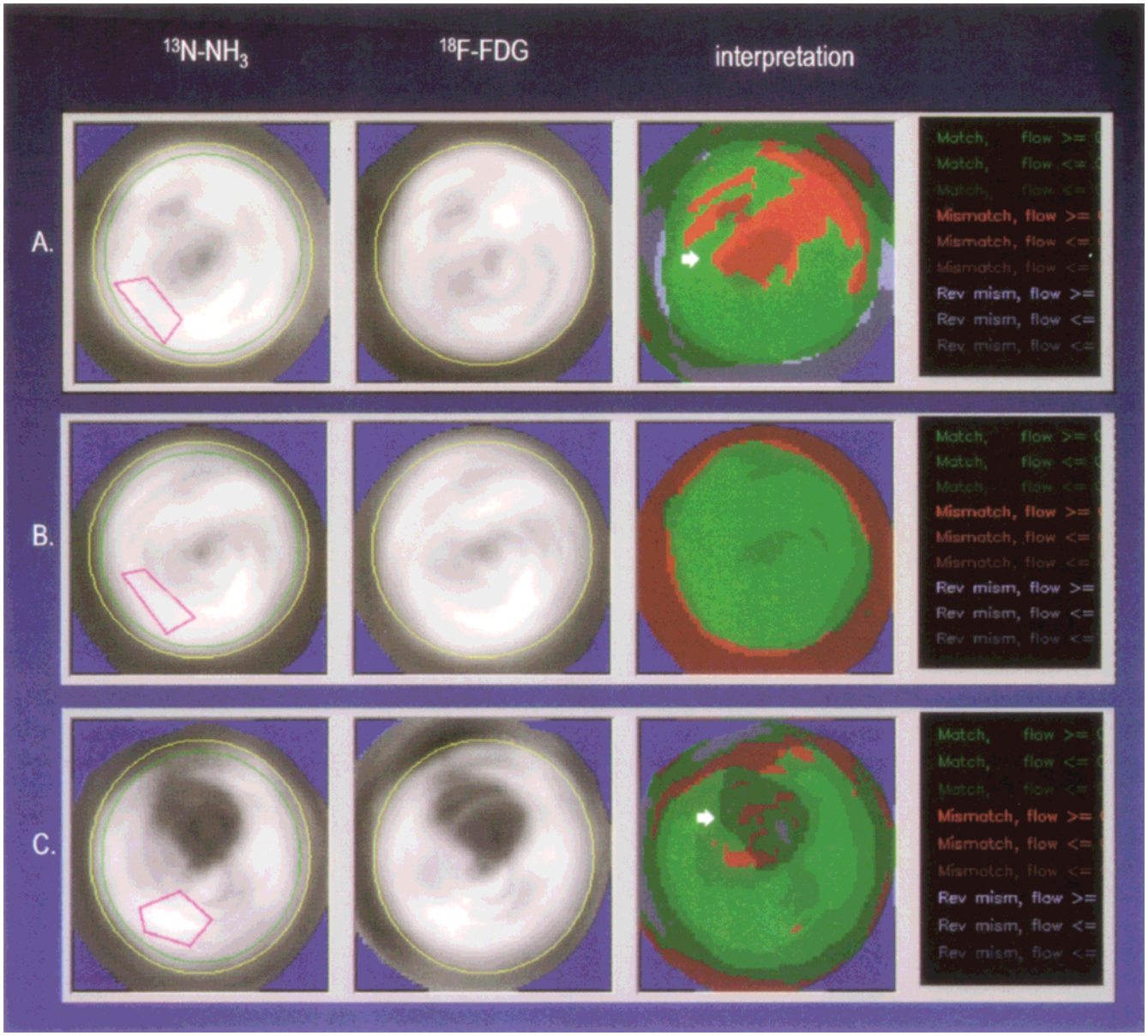

FIGURE 2. Three cases of hypokinesia of the anterior wall. The first map of each case represents the ^{13}N-NH$_3$ uptake, the second the ^{18}F-FDG uptake and the third map is the interpretation image. Relative ^{13}N-NH$_3$ uptake is coded as intensity and the combined patron in color. (A) Decreased flow and preserved metabolism in the anterior wall. The interpretation image shows PET mismatch, represented in red (arrow). The patient had viable myocardial tissue. (B) Normal flow and normal metabolism. The interpretation image shows PET match normal (viable), represented in green. (C) Severely reduced flow and metabolism in the anterior wall. The interpretation shows PET match represented in dark green (arrow). This patient had necrosis of the myocardial tissue that is not viable.

uptake rate in a patient: hyperinsulinemic euglycemic clamping; Acipimox (Pharmacia & Upjohn, Marino Del Tronto, Italy); and oral glucose loading. All studies occur after an overnight fast.

In the hyperinsulinemic euglycemic clamping method, cannulas must be placed in the left and right antecubital veins. One cannula is used for infusing glucose and insulin. The contralateral vein is used to withdraw plasma samples to monitor glucose levels. The insulin infusion rate is adjusted to the patient's weight. Fifty units insulin (0.5 mL) are dissolved in 49.5 mL 0.9% NaCl. A syringe pump is used for the injection. Normal glycemia is obtained with 20% glucose infused at an appropriate rate. Every 5 min a 1-mL blood sample is taken to determine plasma glucose levels. The glucose clamp is optimized during myocardial perfusion imaging. The FDG is injected in a bolus after stabilizing the glucose level between 85 mg% and 95 mg% and not earlier than 50 min after $^{13}NH_3$ injection to allow for ^{13}N decay. The insulin infusion is stopped 15 min before the end of the acquisition.

Clamping is a rather time-consuming and laborious technique. The clamping technique is particularly useful in patients with impaired glucose tolerance or diabetes mellitus, since oral glucose loading frequently results in inadequate image quality in these patients (*59*). Currently we use this technique in our department only for patients with diabetes mellitus and for research protocols.

An alternative approach using a potent nicotinic acid derivative, Acipimox, was introduced because glucose clamping has been suggested to be too complicated for routine clinical use. The principle of this approach is based on the importance of serum FFA concentrations in regulating myocardial glucose uptake. Serum FFA concentrations are strikingly reduced after giving Acipimox leading to enhanced myocardial glucose utilization. Myocardial uptake of glucose is stimulated to the same degree as insulin clamping (*60*).

A cannula is placed in the left antecubital vein to measure plasma glucose. The hyperinsulinemic euglycemic clamping procedure is used if the plasma glucose level is higher than 100 mg%. If the plasma glucose level is below 100 mg%, the patient receives a single dose of 250 mg Acipimox orally, followed by a carbohydrate- and protein-enriched meal. FDG is injected 90 min after the meal. This method is a simple and safe alternative to hyperinsulinemic glucose clamping.

The patient receives 75 g glucose in an aqueous solution, followed by a carbohydrate- and protein-enriched meal, in the oral glucose loading method. The meal must be consumed 30 min after the oral glucose load. FDG is injected 15 min after the meal. After oral glucose loading, glucose levels are significantly higher than during clamping and after Acipimox (*60*). High glucose levels are inversely correlated with image quality.

The static acquisition is started 30 min after injecting FDG if the hyperinsulinemic euglycemic clamping procedure is used. The static acquisition starts 45 min after injecting FDG if either the Acipimox or the oral glucose loading procedures are used. Eight frames are recorded for 5 min each. Total acquisition time is 40 min. The 8 frames of the metabolic PET study are reconstructed using a Hanning 0.4 filter. A summed frame is constructed using all the frames. The creation of radial slices, delineation and polar maps is done in exactly the same way as for flow studies (cfr imaging protocol for ^{13}N-ammonia).

For a dynamic acquisition, glucose levels are controlled using the glucose clamp. The dynamic acquisition starts immediately after injecting the FDG. Dynamic frames are recorded as follows: 8 frames for 15 s each; 4 frames for 30 s each; 2 frames for 1 min each; 2 frames for 2 min each; and 6 frames for 10 min each. Total acquisition time is 70 min.

The 22 frames of the metabolic PET study are reconstructed using a Hanning 0.4 filter. The creation of radial slices is performed as described above. Regional glucose utilization values are estimated by applying a Patlak graphical analysis using frames 8 to 22 (*61*).

Carbon-11-Acetate

Measurement of the oxidation of acetate provides an indirect noninvasive measure of regional oxygen utilization. Initial high uptake of ^{11}C-acetate depends on myocardial blood flow, suggesting that early images may be useful to study myocardial blood flow. After uptake by the myocardium, acetate forms acetyl-CoA to be oxidized in the mitochondria of viable myocytes. Carbon-11 activity is cleared in the form of CO^2. The oxidation of ^{11}C-acetate is suppressed in ischemia. The regional uptake and clearance of ^{11}C-acetate have been used as a noninvasive approach to calculate myocardial oxygen consumption (*62–64*).

Imaging Protocol for Carbon-11-Acetate. A rectilinear and a transaxial transmission scan are performed before each study. Fasting is not necessary. The weight of the patient divided by 4 determines the amount of ^{11}C-acetate with a maximum amount of 20 mCi (740 Mbq) injected. The volume is diluted with 0.9% saline to 5 mL and is injected as a bolus. Dynamic frames are recorded as follows: 8 frames for 30 s each; 6 frames for 60 s each; and 8 frames for 2 min each. The total acquisition time is 26 min.

Polar maps of each of the 22 frames are constructed. Absolute blood flow and oxydative metabolism are calculated using a 3-compartment model (*65,66*).

Collimated and Coincidence Imaging of FDG

PET is an expensive technique and is not available in every department. Two new options for imaging FDG in the myocardium without a PET system have been reported: collimated and coincidence detection. Both can be used to examine myocardial viability. The first method uses 511-keV collimators to image 511-keV photons in a manner similar to SPECT imaging of other radionuclides (*67,68*). The second method uses special electronic circuits on a fully digitized dual-head gamma camera to detect the 511-keV photons, similar to PET with a coincidence circuit (*69,70*). This method is under clinical evaluation in the U.S. and Europe.

The design and construction of modern gamma cameras is optimized for detecting photons in the range of 80–400 keV. Detector shielding is unsuitable for 511-keV photons and, in particular, the thickness of the NaI crystal (scintillator) is insufficient for their efficient detection. Efficiency increases markedly when thicker crystals are used but thicker crystals

TABLE 1
Imaging Patterns Observed With Various Tracers When Viable Myocardial Tissue Is Present

Tracer	Instrumentation	Viable pattern(s)	Nonviable pattern(s)
^{201}Tl (potassium analog)	SPECT Gated SPECT (requires attenuation and scatter correction)	Redistribution Persistent (matched) count defects that demonstrate <25–50% count reduction	Lack of redistribution Persistent (matched) count defects that demonstrate >50% count reduction
^{99m}Tc-sestamibi (perfusion agent)	Gated SPECT (requires attenuation and scatter correction)	Myocardial wall thickening Myocardial wall motion	Lack of myocardial wall thickening Lack of myocardial wall motion
^{123}I-BMIPP (fatty acid analog)	SPECT	Negative mismatch (BMIPP uptake < perfusion agent uptake) The number of mismatched segments is the strongest predictor of future adverse cardiac events	Matched decreased tracer uptake for both BMIPP and a perfusion agent
^{13}N-ammonia (myocardial blood-flow agent)	PET with attenuation correction	PET mismatch (decreased perfusion with FDG uptake)	PET match (decreased perfusion and decreased FDG uptake)
^{18}F-FDG (glucose analog; with glucose uptake rate optimization)	PET with attenuation correction	PET mismatch (decreased perfusion with FDG uptake)	PET match (decreased perfusion and decreased FDG uptake)
^{11}C-acetate (regional myocardial oxygen utilization agent)	PET with attenuation correction	Suppressed clearance (ischemia) or normal clearance following normal uptake	Decreased clearance and uptake No uptake

degrade intrinsic spatial resolution. Ultra-high energy collimators have been developed to permit the imaging of 511-keV photons. These collimators have thicker septa and are considerably heavier than low- and medium-energy collimators. The hole diameter is increased to improve sensitivity and length is increased to maintain reasonable spatial resolution. This form of imaging is restricted to counting photons independently as singles, the line of emission being defined by the collimator characteristics. The disadvantages of this approach are decreased sensitivity and poor resolution (*71*).

The FDG SPECT technique can be used for applications with high tracer uptake, such as in the myocardium. Direct comparisons between FDG SPECT and FDG PET have shown that the assessment of myocardial viability is comparable for both techniques (*72,73*) The 3 methods to optimize the glucose uptake rate in a patient and the injection time of FDG are the same as described above. The same acquisition and reconstruction protocols used for ^{201}Tl scintigraphy can be used for FDG (*73*).

More recently, coincidence detection with a dual-head SPECT scintillation camera has been used to image positron-emitting radionuclides. Converting a double-head gamma camera to perform PET seems to be an excellent, low-cost alternative. The digital detectors of this system have a higher sensitivity and a better resolution than high-energy collimators (*71,74*). Limited data are available about this technique.

CONCLUSION

The differentiation of viable from nonviable myocardial tissue in patients with CAD and LV dysfunction is clinically important. LV function can be improved significantly through various interventions if myocardial tissue is viable. Nuclear medicine techniques, both SPECT and PET, have been described using a variety of tracers and instrumentation. Echocardiography with low-dose dobutamine also can be used to assess myocardial viability.

SPECT techniques use ^{201}Tl, ^{99m}Tc-sestamibi and other perfusion agents. Currently the most widely used free fatty acid analog is ^{123}I-BMIPP. PET techniques are the gold standard for viability studies. PET viability tracers include ^{13}N-ammonia, ^{18}F-FDG and ^{11}C-acetate. The glucose uptake rate must be optimized for ^{18}F-FDG myocardial imaging. Table 1 summarizes the imaging patterns observed when viable myocardial tissue is present.

Instrumentation advances include gated SPECT and coincidence detection. Attenuation and scatter are still characteristics that degrade image quality.

REFERENCES

1. Dilsizian V, Bonow RO. Current diagnostic techniques of assessing myocardial viability in patients with hibernating and stunned myocardium. *Circulation.* 1993; 87:1–20.
2. Braunwald E, Kloner RA. The stunned myocardium: prolonged, postischemic ventricular dysfunction. *Circulation.* 1982; 66:1146–1149.
3. Bolli R. Mechanism of ''myocardial stunning.'' *Circulation.* 1990; 82: 723–738.
4. Marban E. Myocardial stunning and hibernation. The physiology behind the colloquialisms. *Circulation.* 1991; 83:681–688.
5. Bolli R. Myocardial 'stunning' in man. *Circulation.* 1992; 86:1671–1691.
6. Reduto LA, Smalling RW, Freund GC, Gould KL. Intracoronary infusion of streptokinase in patients with acute myocardial infarction: effects of reperfusion on left ventricular performance. *Am J Cardiol.* 1981; 48: 403–409.
7. Nixon JV, Brown CN, Smitherman TC. Identification of transient and persistent segmental wall motion abnormalities in patients with unstable angina by two-dimensional echocardiography. *Circulation.* 1982; 65:1497–1503.
8. Renkin J, Wijns W, Ladha Z, Col J. Reversal of segmental hypokinesis by coronary angioplasty in patients with unstable angina, persistent T wave

inversion, and left anterior descending coronary artery stenosis. Additional evidence for myocardial stunning in humans. *Circulation.* 1990; 82: 913–921.
9. Kloner RA, Allen J, Cox TA, Zheng Y, Ruiz CE. Stunned left ventricular myocardium after exercise treadmill testing in coronary artery disease. *Am J Cardiol.* 1991; 68:329–334.
10. Pfisterer M, Zuber M, Wenzel R, Burkart F. Prolonged myocardial stunning after thrombolysis: can left ventricular function be assessed definitely at hospital discharge? *Eur Heart J.* 1991; 12:214–217.
11. Rahimtoola SH. The hibernating myocardium. *Am Heart J.* 1989; 117: 211–221.
12. Rahimtoola SH. A perspective on the three large multicenter randomized clinical trials of coronary bypass surgery for chronic stable angina. *Circulation.* 1985; 72 (6 pt 2):V123-V135.
13. Braunwald E, Rutherford JD. Reversible ischemic left ventricular dysfunction: evidence for the ''hibernating myocardium.'' *J Am Coll Cardiol.* 1986; 8:1467–1470.
14. Ross J Jr. Myocardial perfusion-contraction matching. Implications for coronary heart disease and hibernation. *Circulation.* 1991; 83:1076–1083.
15. Vanoverschelde JL, Wijns W, Depre C, et al. Mechanisms of chronic regional postischemic dysfunction in humans. New insights from the study of noninfarcted collateral-dependent myocardium. *Circulation.* 1993; 87: 1513–1523.
16. Shen YT, Vatner SF. Mechanism of impaired myocardial function during progressive coronary stenois in conscious pigs. Hibernation versus stunning? *Circ Res.* 1995; 76:479–488.
17. Depre C, Vanoverschelde JL, Melin JA, et al. Structural and metabolic correlates of the reversibility of chronic left ventricular ischemic dysfunction in humans. *Am J Physiol.* 1995; 268 (3 pt 2):H1265-H1275.
18. Cornel JH, Fioretti PM. Assessment of myocardial viability by pharmacological stress echocardiography. In: Van der Wall EE, Blanksma PK, Niemeyer MG, Paans AMJ, eds. *Cardiac Positron Emission Tomography: Viability, Perfusion, Receptors, and Cardiomyopathy.* Dordrecht, Germany: Kluwer Academic Publishers; 1995:103–115.
19. Ragosta M, Beller GA, Watson DD, Kaul S, Gimple LW. Quantitative planar rest-redistribution ^{201}Tl imaging in detection of myocardial viability and prediction of improvement in left ventricular function after coronary bypass surgery in patients with severely depressed left ventricular function. *Circulation.* 1993; 87:1630–1641.
20. Beller GA, Watson DD, Pohost GM. Kinetics of thallium distribution and redistribution: clinical applications in sequential myocardial imaging. In: Strauss HW, Pitt B, eds. *Cardiovascular Nuclear Medicine.* 2nd ed. St. Louis, MO: CV Mosby; 1979:225–242.
21. Johnson LL. Thallium-201 to assess myocardial viability. In: Iskandrian AS, van der Wall EE, eds. *Myocardial Viability: Detection and Clinical Relevance.* Dordrecht, Germany: Kluwer Academic Publishers; 1994: 19–37.
22. Beller GA. Radiopharmaceuticals in nuclear cardiology. In: Beller GA, ed. *Clinical Nuclear Cardiology*. Philadelphia: WB Saunders Co; 1995:37–81.
23. van Eck-Smit BL, van der Wall EE, Siebelink HM, et al. Head-to-head comparison of ^{201}Tl rest-redistribution scintigraphy and stress-immediate reinjection scintigraphy in the detection of myocardial viability. *Nucl Med Commun.* 1996; 17:216–224.
24. Beller GA. Assessment of myocardial viability. In: Beller GA, ed. *Clinical Nuclear Cardiology*. Philadelphia: WB Saunders Co; 1995:293–336.
25. Beanlands RS, Dawood F, Wen WH, et al. Are the kinetics of technetium-99m methoxyisobutyl isonitrile affected by cell metabolism and viability? *Circulation.* 1990; 82:1802–1814.
26. Udelson JE, Coleman PS, Metherall J, et al. Predicting recovery of severe regional ventricular dysfunction. Comparison of resting scintigraphy with ^{201}Tl and ^{99m}Tc-sestamibi. *Circulation.* 1994; 89:2552–2561.
27. Maes AF, Borgers M, Flameng W, Nuyts J, Mortelmans L. Assessment of myocardial viability in chronic coronary artery disease using technetium-99m sestamibi SPECT. Correlation with histologic and positron emission tomographic studies and functional follow-up. *J Am Coll Cardiol.* 1997; 29:62–68.
28. Germano G, Kiat H, Kavanagh PB, et al. Automatic quantification of ejection fraction from gated myocardial perfusion SPECT. *J Nucl Med.* 1995; 36:2138–47.
29. Depuey EG, Nichols K, Dobrinsky C. Left ventricular ejection fraction assessed from gated technetium-99m-sestamibi SPECT. *J Nucl Med.* 1993; 34:1871–1876.
30. Germano G, Erel J, Lewin H, Kavanagh P, Berman D. Automatic quantitation of regional myocardial wall motion and thickening from gated technetium-99m sestamibi myocardial perfusion single-photon emission computed tomography. *J Am Coll Cardiol.* 1997; 30:1360–1367.
31. Nuyts J, Dupont P, Van den Maegdenbergh V, et al. A study of the liver-heart artifact in emission tomography. *J Nucl Med.* 1995; 36:133–139.
32. Manglos SH, Thomas FD, Gagne GM, Hellwig B. Phantom study of breast tissue attenuation in myocardial imaging. *J Nucl Med.* 1993; 34:992–996.
33. Matsunari I, Boning G, Ziegler SI, et al. Effects of misalignment between transmission and emission scans on attenuation-corrected cardiac SPECT. *J Nucl Med.* 1998; 39:411–416.
34. Galt JR, Cullom SJ, Garcia EV. SPECT quantification : a simplified method of attenuation and scatter correction for cardiac imaging. *J Nucl Med.* 1992; 33:2232–2237.
35. Ficaro EP, Fessler JA, Ackermann RJ, et al. Simultaneous transmission-emission thallium-201 cardiac SPECT: effect of attenuation correction on myocardial tracer distribution. *J Nucl Med.* 1995; 36:921–931.
36. Hutton BF. Cardiac single-photon emission tomography: is attenuation correction enough? *Eur J Nucl Med.* 1997; 24:713–715.
37. King MA, Hademenos GJ, Glick SJ. A dual-photopeak window method for scatter correction. *J Nucl Med.* 1992; 33:605–612.
38. Fujibayashi Y, Yonekura Y, Takemura Y, et al. Myocardial accumulation of iodinated beta-methyl-branched fatty acid analog, iodine-125–15-(p-iodophenyl)-3-(R,S) methyl-pentadecanoic acid (BMIPP), in relation to ATP concentration. *J Nucl Med*. 1990; 31:1818–1822.
39. Knapp FF Jr, Ambrose KR, Goodman MM. New radioiodinated methyl-branched fatty acids for cardiac studies. *Eur J Nucl Med.* 1986; 12 (suppl):S39–S44.
40. Matsunari I, Saga T, Taki J, et al. Kinetics of iodine-123-BMIPP in patients with prior myocardial infarction: assessment with dynamic rest and stress images compared with stress thallium-201 SPECT. *J Nucl Med.* 1994; 35:1279–1285.
41. Tateno M, Tamaki N, Yukihiro M, et al. Assessment of fatty acid uptake in ischemic heart disease without myocardial infarction. *J Nucl Med.* 1996; 37:1981–1985.
42. Kobayashi H, Kusakake K, Momose M, et al. Evaluation of myocardial perfusion and fatty acid uptake using a single injection of iodine-123-BMIPP in patients with acute coronary syndromes. *J Nucl Med.* 1998; 39:1117–1122.
43. Franken PR, Dendale P, De Geeter F, et al. Prediction of functional outcome after myocardial infarction using BMIPP and sestamibi scintigraphy. *J Nucl Med.* 1996; 37:718–722.
44. Tamaki N, Tadamura E, Kudoh T, et al. Prognostic value of iodine-123 labelled BMIPP fatty acid analogue imaging in patients with myocardial infarction. *Eur J Nucl Med.* 1996; 23:272–279.
45. Hambye A-SE, Vaerenberg MM, Dobbeleir AA, Van den Heuvel PA, Franken PR. Abnormal BMIPP uptake in chronically dysfunctional myocardial segments: correlation with contractile response to low-dose dobutamine. *J Nucl Med.* 1998; 39:1845–1850.
46. De Geeter F, Franken PR, Knapp FF Jr, Bossuyt A. Relationship between blood flow and fatty acid metabolism in subacute myocardial infarction: a study by means of ^{99m}Tc-sestamibi and ^{123}I-beta-methyl-iodo-phenyl pentadecanoic acid. *Eur J Nucl Med.* 1994; 21:283–291.
47. Tamaki N, Kawamoto M, Yonekura Y, et al. Assessment of fatty acid metabolism using I-123 branched fatty acid: comparison with positron emission tomography. *Ann Nucl Med.* 1993; 7 (suppl):SII 41-SII 47.
48. De Geeter F, Franken PR, Defrise M, et al. Optimal collimator choice for sequential iodine-123 and technetium-99m imaging. *Eur J Nucl Med.* 1996; 23:768–774.
49. Dobbeleir AA, Hambye AS, Franken PR. Influence of methodology on the presence and extent of mismatching between ^{99m}Tc-MIBI and ^{123}I-BMIPP in myocardial viability studies. *J Nucl Med.* 1999;40:in press.
50. Schwaiger M, Hicks R. The clinical role of metabolic imaging of the heart by positron emission tomography. *J Nucl Med.* 1991; 32:565–578.
51. Maes A, Mortelmans L, Nuyts J, et al. Importance of flow/metabolism studies in predicting late recovery of function following reperfusion in patients with acute myocardial infarction. *Eur Heart J.* 1997; 18:954–962.
52. Nuyts J, Suetens P, Oosterlinck A, De Roo M, Mortelmans. Delineation of ECT images using global constraints and dynamic programming. *IEEE Trans Med Imaging.* 1991; 10:489–498.
53. Maes A, Flameng W, Nuyts J, et al. Histological alterations in chronically hypoperfused myocardium. Correlation with PET findings. *Circulation.* 1994; 90:735–745.
54. Hutchins GD, Schwaiger M, Rosenspire KC, et al. Noninvasive quantification of regional blood flow in the human heart using N-13 ammonia and dynamic positron emission tomographic imaging. *J Am Coll Cardiol.* 1990; 15:1032–1042.
55. Muzik O, Beanlands RS, Hutchins G, et al. Validation of nitrogen-13-ammonia tracer kinetic model for quantification of myocardial blood flow using PET. *J Nucl Med*. 1993; 34:83–91.

56. Liedtke AJ. Alterations of carbohydrate and lipid metabolism in the acutely ischemic heart. *Prog Cardiovasc Dis.* 1981; 23:321–336.
57. Camici P, Ferrannini E, Opie LH. Myocardial metabolism in ischemic heart disease: basic principles and application to imaging by positron emission tomography. *Prog Cardiovasc Dis.* 1989; 32:217–238.
58. Eitzman D, Al-Aouar Z, Kanter HL, et al. Clinical outcome of patients with advanced coronary artery disease after viability studies with positron emission tomography. *J Am Coll Cardiol.* 1992; 20:559–565.
59. Knuuti MJ, Nuutila P, Ruotsalainen U, et al. Euglycemic hyperinsulinemic clamp and oral glucose load in stimulating myocardial glucose utilization during positron emission tomography. *J Nucl Med.* 1992; 33:1255–1262.
60. Bax JJ, Veening MA, Visser FC, et al. Optimal metabolic conditions during fluorine-18 fluorodeoxyglucose imaging; a comparartive study using different protocols. *Eur J Nucl Med.* 1997; 24:35–41.
61. Patlak CS, Blasberg RG. Graphical evaluation of blood-to-brain transfer constants from multiple-time uptake data. Generalizations. *J Cereb Blood Flow Metab.* 1985; 5:584–590.
62. Chan SY, Brunken RC, Phelps ME, Schelbert H. Use of the metabolic tracer carbon-11-acetate for evaluation of regional myocardial perfusion. *J Nucl Med.* 1991; 32:665–672.
63. Gropler RJ, Siegel BA, Geltman EM. Myocardial uptake of carbon-11-acetate as an indirect estimate of regional myocardial blood flow. *J Nucl Med.* 1991; 32:245–251.
64. Brown MA, Myears DW, Bergmann SR. Validity of estimates of myocardial oxidative metabolism with carbon-11-acetate and positron emission tomography despite altered patterns of substrate utilization. *J Nucl Med.* 1989; 30:187–193.
65. Buck A, Wolpers HG, Hutchins GD, et al. Effect of carbon-11-acetate circulation on estimates of myocardial oxygen consumption by PET. *J Nucl Med.* 1991; 32:1950–1957.
66. Chen K, Huang SC, Feng D. New estimation methods that directly use the time accumulated counts in the input function in quantitative dynamic PET studies. *Phys Med Biol.* 1994; 39:2073–2090.
67. Martin WH, Delbeke D, Patton JA, et al. FDG SPECT: correlation with FDG PET. *J Nucl Med.* 1995; 36:988–995.
68. Van Lingen A, Huijgens PC, Visser FC, et al. Performance characteristics of a 511-keV collimator for imaging positron emitters with a standard gamma camera. *Eur J Nucl Med.* 1992; 19:15–21.
69. Drane WE, Abbott FD, Nicole MW, Mastin S, Kuperus J. Technology for FDG SPECT with a relatively inexpensive gamma camera. Work in progress. *Radiology.* 1994; 191:461–465.
70. Mertens JD, Bhend WL. Digital coincidence detection: a scanning VLSI implementation. *IEEE Nucl S.* 1993; 40:2037–2039.
71. Abdel-Dayem HM, Radin AI, Luo JQ, et al. Fluorine-18-fluorodeoxyglucose dual-head gamma camera coincidence imaging of colorectal carcinoma. *J Nucl Med.* 1998; 39:654–656.
72. Jarritt PH, Acton PD. PET imaging using gamma camera systems: a review. *Nucl Med Commun.* 1996; 17:758–766.
73. Bax JJ, Visser FC, van Lingen A, et al. Feasibility of assessing regional myocardial uptake of ^{18}F-fluorodeoxyglucose using single photon emission computed tomography. *Eur Heart J.* 1993; 14:1675–1682.
74. Stokkel MP, Terhaard CH, Mertens IJ, Hordijk G, van Rijk P. Fluorine-18-FDG detection of laryngeal cancer postradiotherapy using dual-head coincidence imaging. *J Nucl Med.* 1998; 39:1385–1387.